On-line monitoring of composite nanoparticles synthesized in a pre-industrial laser pyrolysis reactor using Laser-Induced Breakdown Spectroscopy

Tanguy Amodeo, Christophe Dutouquet, François Tenegal, Benoît Guizard, Hicham Maskrot, Olivier Le Bihan, Emeric Frejafon

On-line monitoring of composite nanoparticles synthesized in a pre-industrial laser pyrolysis reactor using Laser-Induced Breakdown Spectroscopy (LIBS)

Tanguy Amodeo[a], Christophe Dutouquet[a], François Tenegal[b], Benoît Guizard[b], Hicham Maskrot[b], Olivier Le Bihan[a] and Emeric Fréjafon[a]

[a] Institut National de l'Environnement Industriel et des Risques (INERIS), Parc Technologique Alata, BP2, 60550 Verneuil-En-Halatte, France

christophe.dutouquet@ineris.fr, olivier.le-bihan@ineris.fr, emeric.frejafon@ineris.fr

[b] DEN / DMN / SRMA / LTMEx, CEA Saclay, 91191 Gif Sur Yvette, France

francois.tenegal@cea.fr, benoit.guizard@cea.fr, hicham.maskrot@cea.fr

Corresponding author:

Tanguy Amodeo

Phone: +33 (0) 3 44 55 69 47

Fax: + 33 (0) 3 44 55 63 02

Email address: tanguy.amodeo@ineris.fr

Abstract

Laser-Induced Breakdown Spectroscopy (LIBS) was employed for on-line and real time process monitoring during nanoparticle production by laser pyrolysis. Laser pyrolysis has proved to be a reliable and versatile method for nanoparticle production. However, an on-line and real time monitoring system could greatly enhance the process optimization and accordingly improve its performances. For this purpose, experiments aiming at demonstrating the feasibility of an on-line monitoring system for silicon carbide nanoparticle production using the LIBS technique were carried out. Nanosecond laser pulses were focused into a cell through which part of the nanoparticle flux diverted from the production process was flowed for LIBS analysis purposes. The nanoparticles were vaporized within the laser-induced plasma created in argon used as background gas in the process. Temporally-resolved emission spectroscopy measurements were performed in order to monitor nanoparticle stoichiometry. Promising results were obtained and on-line Si/C_X stoichiometry was successfully observed. These results put forward the possibility of real time correction of the nanoparticle stoichiometry during the production process.

Key words

LIBS, on-line monitoring, process control, laser pyrolysis, composite nanoparticles

1. Introduction

Over the last years, research in the field of nanostructured materials synthesis has become increasingly important. Such materials designed at a nanometric scale are expected to show new properties of great interest to a wide range of industrial applications. In this context, the development of nanoparticle-based materials has advanced rapidly and along with it the need for generic and safe nanoparticle production systems. Producing and commercializing nanoparticle-based materials for different applications (composites, cosmetics, catalysis, optics,…) require industrial equipments permitting large-scale production of a wide range of nanoparticles. Furthermore, these industrial lines are expected to produce nanoparticles with constant quality (size distribution, chemical composition).

For this purpose, the development of an on-line monitoring system allowing a real time analysis, both qualitative and quantitative, of some characteristics of the nanoparticles such as the chemical composition and the size is highly desirable. The monitoring of some of these characteristics will thus provide quasi instantaneous feedback for process control. This is of primary importance while the development of composite nanoparticles arouses a growing interest. These nanoparticles are elaborated from several elements with the aim of creating materials with advanced functionalities. The large number of elements these nanoparticles consist of has actually emphasized the need for on-line stoichiometry control. In addition to process control, production safety requirements could be satisfied by utilizing on-line monitoring systems to secure the installations producing, handling and integrating nanoparticles. A tool devised both for in-situ and real time chemical and physical identification of nanoparticles could detect their release in the ambient air and therefore could assure safety for the operating personnel and the surrounding environment.

Among all the methods known, the continuous nanoparticle synthesis processes are very interesting for nanoparticle production at industrial scale. Indeed, with these techniques, nanoparticles are produced continuously by injecting a continuous flow of reactants in a reactor leading to large daily production rates. Some of these methods are already developed at industrial scale for the production of metals or oxides nanoparticles (for example TiO_2 nanoparticles by the Aerosil® process of DEGUSSA) and the development of industrial processes for non-oxide nanoparticles is currently in progress. Laser pyrolysis is one of these promising techniques. Basically, its principle rests on the interaction between a continuous high-power CO_2 laser beam and a continuous flux of gaseous or liquid reactants. Reactant

molecules absorb laser radiation which results in their dissociation. Afterwards, molecules recombine with one another within the pyrolysis flame to form nanoparticles. Thereby, a wide range of nanoparticles can be produced. The process yields a continuous high production rate of nanoparticles with a good control of their size, structure and chemical composition [1]. Furthermore, nanoparticles produced in this way are usually weakly agglomerated. In addition, the method is very efficient to produce composite nanoparticles which characteristics can be easily adjusted by varying some processing parameters such as the laser power density, the flow rate, the composition and dilution of the reactants.

Though this method assures a good control of compound stoichiometry, stoichiometry variations in the course of nanoparticle production are not to be neglected. Thus, the production rate of nanoparticle compounds with the right stoichiometry could be enhanced with an on-line and real time quality control. With this aim in view, the LIBS technique was selected. LIBS has been demonstrated to be a versatile, reliable analytical method for multi-elemental analysis of solid [2], liquid [3], gas [4,5] and aerosols [6,7] both for qualitative and quantitative measurements. It has the advantage of being non-intrusive and no sampling is required. Moreover, measurements can be performed at remote distances, in real time and in-situ without sample preparation. All these characteristics make LIBS a particularly well adapted tool to analyze materials which are not easily accessible or for which confinement is required.

The LIBS analysis method has already been utilized in diverse industrial applications. Its potential in the steel industry at different stages of the production chain has already been demonstrated [8,9]. For instance, the LIBS technique has been applied for on-line monitoring of molten steel in order to improve the steel quality and to obtain a better production gain. In the nuclear industry [10], LIBS has been selected as the most adequate technique when in-situ material analyses were required. It was the most practical method to implement in a hostile environment with high temperatures and level of radiation. Recently, concerns have been raised regarding particles of micrometric and submicrometric sizes emitted in ambient air (from different sources such as plants, engines….) and their possible hazard towards human health and environment. Several studies have demonstrated the LIBS potentialities for particle detection [11]. LIBS was therefore used for on-line monitoring of metal laden aerosols in industrial production, combustion processes [12,13,14], environmental purposes [15,16] and promising results were obtained. All these studies point out the advantages of LIBS for process control and particle detection both on-line and in real time.

In this paper, we report the results of a study coupling for the first time the LIBS technique and a laser pyrolysis reactor. The LIBS equipment was integrated into a laser pyrolysis unit developed by the French Atomic Energy Commission (CEA – Saclay, France) with the aim of monitoring on-line and in real time SiC_X composite nanoparticle stoichiometry. These nanoparticles are synthesized prior to nanostructured silicon carbide elaboration, the latter being a promising material for high temperature applications in the nuclear energy industry. Our main objective was centred on nanoparticle stoichiometry determination while the process was being operated. Stoichiometry calculation was achieved using temporally-resolved emission spectroscopy measurements followed by plasma analysis. The results obtained are reported and discussed.

2. Experimental set-up: LIBS & laser pyrolysis

2.1 Instrumentation

2.1.1 Laser pyrolysis experimental set-up

The experimental set-up (figure 1) consists of a reactor equipped with an inlet nozzle at its bottom, an outlet duct at its top and many optical windows among which those for the laser beam passage and the pyrolysis flame monitoring. Reactants, namely SiH_4 and C_2H_2 for SiC_X nanoparticle synthesizing are admitted in the pyrolysis reactor through the inlet nozzle, the latter being flat or cylindrical. Reactants can be injected with different flow rates. A continuous high-power CO_2 laser beam is expanded to twice its starting diameter with an optical system and focused in the vertical direction using a 500 mm focal length zinc-selenium (ZnSe) cylindrical lens. The resulting 30 mm width elliptical cross-section beam passes through the reactor perpendicularly to the above mentioned reactant jet coming out from the nozzle. A wide range of laser power density values for reactant irradiation are accessible by adjusting the distance between the cylindrical lens and the nozzle. The position of maximum focusing is attained for a distance between the cylindrical focusing lens and the nozzle matching the lens focal length and corresponds to the maximum irradiance of 50 kW/cm^2. A co-flow of argon gas is injected around the reactants in order to confine the reaction. At the same time, a stream of argon sweeps all the inner window surfaces to avoid particle deposition. Eventually, the nanoparticles are evacuated from the reactor with argon as a carrier gas. Then, they are directed towards the nanoparticle collector thanks to a pump placed downstream of the collector and connected to an exhaust-treatment system constituted of a

scrubber and a washer. It should be noted that the production rate of this unit can go beyond 1 kg of silicon carbide (SiC) nanoparticles per hour.

2.1.2 LIBS experimental set-up

The experimental set-up of the LIBS system mounted on the laser pyrolysis process is depicted on figure 2. In order to carry out the LIBS experiment, a metallic flow cell devoted to LIBS analysis through which part of the nanoparticle flow was diverted was installed on the process. A bypass line was specially designed to achieve this diversion and to enable an on-line continuous sampling from the main stream of nanoparticles. Using the bypass line, the inlet end of the cell was connected to the nanoparticle production conduit upstream of the nanoparticle collector. The outlet end was linked to the exhaust conduit downstream of the collector. The pre-existent pressure difference between the two connection points sufficed to make the nanoparticles carried by the argon gas stream circulate through the cell for LIBS analysis purposes. A small filter collector was placed downstream of the cell outlet to prevent the particles from being released in the main line. A laser pulse of 5 ns duration and 50 mJ energy originating from a Q-switched Nd-Yag laser (λ = 1064 nm) operated at 20 Hz was focused inside the cell using a fused silica plano-convex lens of 50 mm focal length the cell was fitted with. The resulting beam waist value was about 100 µm leading to an estimated fluence value of 150 J cm^{-2} at the focal point. The LIBS signal originating from the plasma created in the argon-nanoparticle mixture was collected through a quartz window perpendicularly to the LIBS laser beam with a telescope of 150 mm focal length. The plasma emission was imaged onto the entrance a 50 µm diameter core optical fiber. The fiber was linked to an Echelle spectrometer (Mechelle 5000, resolution of 0.1 nm at 500 nm) equipped with a fast intensified CCD camera (Andor Istar, model DH734-18F-03).

2.2 Nanoparticle synthesizing parameters

The LIBS experiments planned required nanoparticle stoichiometry and concentration to vary. Table 1 reports the parameters used to produce nanoparticles for this study. The experiments were carried out with a defocused beam (-150 mm) corresponding to an energy of 420 W/cm^2. The relative flow rates of SiH_4 and C_2H_2 were set so that nanoparticles having the following theoretical stoichiometries SiC, SiC_2, SiC_4 and SiC_8 could be synthesized, the chemical yield for laser pyrolysis experiments using

mixtures of SiH_4 and C_2H_2 being close to 1 (all Si and C atoms are recovered in a condensed form) [17]. The mass concentration was varied from 1.6 to 11.2 μg per cm^3 by changing the ratio between the reactants flow rate and the argon flow rate. The production rate in mass was calculated considering a chemical yield of 1 for all the conditions.

3. Foreword: stoichiometry

Stoichiometry determination requires to establish a relationship between the measured spectroscopic intensities and the densities of the different elements the nanoparticles consisted of prior to vaporization. A simple equation links the measured intensity ratios to the elemental density ratios provided several conditions are fulfilled. The plasma has to be in local thermal equilibrium state (LTE) and optically thin for the transitions observed. If these conditions are met, the equation yielding stoichiometry *S* by relating the integrated intensity ratio to the density ratio writes

$$S = \frac{N_{Tot}^{a}}{N_{Tot}^{b}} = \frac{I_{ij}^{a}\,\lambda_{ij}^{a}\,Z^{a}\,g_k\,A_{kl}^{b}}{I_{kl}^{b}\,\lambda_{kl}^{b}\,Z^{b}\,g_i\,A_{ij}^{a}} \quad \exp\left[-\frac{E_k^b - E_i^a}{kT_e}\right] \tag{1}$$

where *a* and *b* are the elements studied, *ij* and *kl* the selected transitions for *a* and *b* elements respectively, I_{ij}^{a} and I_{kl}^{b} the measured integrated intensities, λ_{ijl}^{a} and λ_{kl}^{b} the wavelength of the selected transitions, Z^{a} and Z^{b} the partition functions of a and b elements in a given ionization stage, g_i et g_k statistical weight of upper states with the corresponding E_i^a and E_k^b energies, A_{ij}^{a} and A_{kl}^{b} transition probabilities, N^{a} and N^{b} total number of a and b atoms in a given ionization stage and T_e the electronic temperature.

Basically, stoichiometry determination consists of measuring the ratio of the total number of atoms of each element. With the above formula, only ratios of total number of atoms in a given ionization stage is accessible. Nevertheless, stoichiometry can be inferred from ratio of total number of atoms in the neutral state on the condition that the ion density be negligible compared to that of neutral density. Temporally-resolved emission spectroscopy allows the determination of the right temporal window matching this criterion and the other two: LTE and optically thin plasma. In the paragraphs to follow, a brief description of our time-resolved spectroscopic measurements will be presented. LTE validity will be

discussed and the electronic temperature calculated. Finally, plasma optical thickness will be examined and stoichiometry results will be presented and discussed.

4. Results

4.1 Lines identification

In order to identify all the emitting species of interest vaporised within the plasma and to determine the best recording parameters for stoichiometry determination, time-resolved spectroscopic measurements were carried out. Series of spectra were recorded as a function of time delay (t_d) and ICCD gate width. Two series of measurements corresponding to two ranges of time delay were performed. In the first series a 100 ns ICCD gating time was chosen with time delay varying from 200 ns to 2.2 µs. In the second series, the time delay was varied from 2.2 µs to 60 µs using a gate width of 2 µs. In order to enhance the signal-to-background ratio, spectra were accumulated over several laser-induced spark events. Each spectrum consisted of an accumulation of 400 and 200 laser shots for the first and second series respectively. The same recording parameters were used during the vaporisation of nanoparticles with different stoichiometry (Si, SiC, SiC_2, SiC_4 and SiC_8). Lines identification was performed using the NIST [18] database.

In the early times of the laser spark event (200 ns < t_d < 2 µs), many widened argon lines were detected up to approximately 2 µs delay time. The strongly widened H_α line at 656.279 nm originating from the laser pyrolysis reaction also appeared in the spectra. The strong line widening observed is characteristic of Stark broadening and suggests a high electronic density in the early times of plasma expansion. Singly ionised Ar and Si ions (Ar II at 480.602 nm and Si II at 385.602 nm, 386.26 nm, 412.807 nm, 413.089 nm, 504.103 nm, 505,598 nm, 634.71 nm and 637.13 nm) were identified. Line intensities of these ions decreased rapidly due to plasma recombination. These ions were no longer visible beyond 2 µs time delay. No carbon ions were seen in the recorded spectra. Many neutral Ar and Si lines were detected with a good signal-to-background ratio and their intensity lines increased with decreasing ion concentration. Neutral carbon is usually not easily detected because of its low transition probability values. Thus, only the strongest C line at 247.85 nm was observed during our measurements. Figure 3 shows a spectrum recorded (time delay 4.2 µs, ICCD gate width 2 µs) during vaporisation of SiC_2 nanoparticles within the plasma created in argon as background gas. The nanoparticle concentration value

was calculated to be 5.3 µg per cubic centimetres according to table 1. The carbon line at 247.85 nm and six Si lines were clearly identified. Many argon lines were identified and used for plasma analysis purposes both for electronic temperature and density measurements. For time delay beyond approximately 8 µs, molecule formation of C_2 was observed. No other molecule formation was detected.

4.2 Plasma analysis

4.2.1 Electronic density

The temporal evolution of the electronic density was obtained from Stark broadening measurements. The electronic density was calculated by fitting computed spectra with experimental data. In the early times of the laser spark event, the plasma is highly ionized and Stark broadening dominates over other broadening effects. Spectral line shapes were then simulated using Lorentzian profiles for these functions are well suited to approximate Stark broadened lines [19]. For usual LIBS conditions, one generally assumes ion contribution to Stark broadening is negligible which results in the simplifying of the Stark width expression [20]. A linear dependence of the Stark width on the electronic density N_e was then assumed for the calculations according to the well known formula

$$\Delta\lambda_{Stark} \approx 2W_{ref}\left(\frac{N_e}{N_e^{ref}}\right) \tag{2}$$

In the above equation, $\Delta\lambda_{Stark}$ is the measured Stark width (FWHM), W_{ref} is the half width at half-maximum Stark parameter for a given electron density N_e^{ref}. The apparatus width of the spectrometer was measured using a mercury-argon calibration lamp. The 750.386 and 751.465 nm argon lines and the H_α line at 656.279 nm were chosen for electronic density determination for Stark widths of these lines have well known tabulated values [21, 22]. Figure 4 shows an experimental spectrum recorded with a 4.2 µs time delay and a 2 µs gate width and compared with a simulated profile. The computed spectrum fits the experimental profile very well for an electronic density value of 9 10^{16} cm^{-3}. Seventy percent of the values measured using the H_α line fall within the range of 20 to 50 percent agreement with those obtained from argon lines. The rest of the points scores badly within the range of 50 to 90 percent agreement. Figure 5 presents the temporal evolution of the electronic density during SiC and SiC_8 nanoparticle vaporization. No significant differences of electronic densities were observed for both

stoichiometries. Electronic density values of SiC and SiC_8 are almost identical for time delays ranging from 2 µs to 10 µs. For time delays inferior to 2 µs, the slight densitydifference could be accounted for by the difficulty encountered when simulating strongly widened experimental lines appearing in the early times of the plasma formation.

4.2.2 Electronic temperature

The electronic temperature was calculated using Boltzmann plot method based on the following equation

$$\ln\left[\frac{I_{nm}\,\lambda_{nm}}{g_n\,A_{nm}}\right] = -\frac{E_n}{k\,T_e} + C \qquad (3)$$

n and *m* being the upper and lower levels of the selected transition respectively, I_{nm} the integrated intensity of the transition, λ_{nm} its wavelength, g_n statistical weight of the upper state level, A_{nm} transition probability, E_n energy of the upper state level, T_e the electronic temperature, *k* Boltzmann constant, and *C* a constant.

The 17 strong argon lines which were chosen for the Boltzmann plots are listed in table 2. In order to carry out calculations using different spectral regions, the Echelle / ICCD system was calibrated with a deuterium tungsten-halogen light source (DH-2000-CAL, Ocean Optics). The blackbody radiation emitted from the lamp allowed calibration of the acquired spectra. The calculations are therefore more precise for this calibration gives access to a wide range of lines with different upper energy levels. One of the Boltzmann plot used for temperature determination is displayed in figure 6. The evolution of the plasma temperature is shown in figure 7 as a function of time delay when irradiating SiC nanoparticles. It should be noted that the electronic temperature did not show a great sensitivity to stoichiometry and concentration variations within the ranges investigated.

4.2.3 LTE validity

Plasmas with high electronic densities (namely, electronic densities superior to 10^{16} cm^{-3}) such as laser-induced plasmas are very close to the local thermal equilibrium (LTE). The assumption of LTE is usually made for laser generated plasmas obtained in air or argon at atmospheric pressure [23]. Usually,

the LTE validity verification consists of calculating the lower limit of electron density N_L for the LTE to be established according to a criterion such as the Mac Whirter criterion:

$$N_e > N_L = 1.6\,10^{12}\sqrt{T_e}\,(\Delta E)^3 \quad (4)$$

where ΔE is the highest energy difference between upper and lower energy levels (eV) populated according to LTE conditions and between which a transition is possible. For the calculation of N_L, the chosen electronic temperature value corresponded to the maximum time delay of 10 µs for which electronic density could be measured, that is to say, a value of around 12300 K according to figure 7. The upper and lower energy levels of the 419.10 nm argon line match the above criteria for the evaluation of ΔE which value equals therefore 2.95 eV according to table 2. Eventually, N_L value was found to be 4.5 10^{15} cm^{-3}. According to the electronic density graph of figure 5, LTE validity is therefore established for time delay below 10 µs. Beyond this delay range, electronic density measurement became uneasy as Stark broadening effect was diminishing.

4.2.4 Temporal window choice

Equation (1) allowing stoichiometry calculation only applies under LTE conditions. The LTE criterion was found to be fulfilled for time delay values under 10 µs. For reasons explained previously (3), ion density must be negligible compared to that of neutrals for equation (1) to be applied. Temporal evolution of lines emitted from the plasma showed that no ion emission was detected for time delays higher than 2µs. Total number of Si and C ions are therefore assumed to be negligible and stoichiometry determination can be achieved using equation (1). The best Boltzmann's plots were obtained for a time delay of 4.2 µs which eventually resulted in our selecting this value for all our stoichiometry measurements.

4.3 Stoichiometry calculation. Discussion

Stoichiometry was evaluated in accordance with equation (1) taking into account the above plasma analysis results. Two lines had to be chosen for stoichiometry calculation. As explained in section (4.1), carbon line at 247 nm was the only neutral carbon line available on all the spectra recorded and was therefore automatically chosen. The Si line at 288.157 nm was selected for two reasons. It had a better signal-to-background ratio than the other detected transitions. Furthermore, its repeatability proved to be higher than the other recorded lines. Spectroscopic characteristics of these lines are reported in table 3. The strong transition probability of the aforementioned Si line makes it prone to self absorption. With the

aim of verifying whether it was subject to self absorption, a flow of nanoparticles containing only the Si element was produced and analyzed. The LIBS intensity of this Si line was studied as a function of nanoparticle concentration. To this end, the spectra were recorded with the above selected delay of 4.2 µs but with an extended gate width of 20 µs. A fast analysis of all the Si spectra did not reveal any signs of strong self absorption. No self-reversed lines were observed. Figure 8 shows a graph representing the 288.157 nm Si line intensity evolution as a function of concentration. Its intensity proved to be linear within the concentration range investigated. This result points out that self absorption was virtually non-existent under our experimental conditions. Self absorption of C line was assumed to be negligible as its transition probability was weaker than that of Si at 288.157 nm. These results account for the optically thin plasma hypothesis necessary for equation (1) to be applied.

Plotting such graph also aimed at detecting possible saturation of the LIBS signal which may have occurred in case of incomplete nanoparticle vaporization within the plasma. Usually, the grain size of nanoparticles varies within a range of 20 to 100 nanometers when produced by laser pyrolysis. Carranza and Hahn demonstrated incomplete vaporization of micrometric-sized particles even for high laser irradiance and concluded the existence of an upper particle size of 2.1 µm beyond which vaporization was not completed [24]. In addition, possible depletion of nanometric-sized particles from the plasma core was also reported [25]. Previous experiments carried out in our laboratory at INERIS showed linear dependence of LIBS intensity on particle sizes ranging from 40 nm to 500 nm while irradiating NaCl particles under comparable experimental conditions. In the present work, the detected LIBS intensity showed a linear dependence both on concentration and particle size.

Eventually, all the criteria necessary for proper use of equation (1) were fulfilled. Stoichiometry was calculated with a 4.2 µs time delay recorded spectra and a 2 µs gate width as stated in 4.2.4. The results obtained are reported in table 4 and are in good accordance with the known theoretical values. However, calculations performed with equation (1) suggest that stoichiometry determination can be strongly temperature dependent. This is evidenced by writing stoichiometry relative uncertainty

$$\frac{\Delta S}{S} = \frac{\Delta\left(I_{ij}^{a} / I_{kl}^{b}\right)}{I_{ij}^{a} / I_{kl}^{b}} + \frac{\left|E_i^a - E_k^b\right|}{k T_e} \frac{\Delta T_e}{T_e} \tag{5}$$

The first term in equation (5) is related to relative errors on line ratio measurements including implicitly different uncertainties such as spectra repeatability and potential self-absorption

underestimation. These experiments pointed out that repeatability increased with increasing of number of accumulated spectra, as often verified in LIBS experiments. However our experiments had to be carried out in the allotted time corresponding to the reactor availability. For this first laser pyrolysis reactor – LIBS coupling, temporally-resolved emission spectroscopy measurements were performed. These experiments carried out for different stoichiometry and concentration were time consuming and did not lead us to record spectra with a large number of accumulations. Spectra corresponding to the selected temporal window and recorded with a larger number of accumulations could have enhanced our results.

One characteristic of the LIBS technique applied to particle analysis is the particle presence probability within the laser-induced plasma. For low micrometric-sized particle concentration values such as a few micrograms per cubic meters, it has been demonstrated that a particle hit (a particle vaporized within the plasma and leading to LIBS detection) could be modeled with a Poisson probability law [26]. Thus, the laser-induced plasma corresponding to one shot may be ignited without any particle of the analyte passing through the plasma volume. No spectroscopic signal is then recorded for that shot lowering thereby the signal-to-background ratio of the resulting spectrum and its repeatability. Under our experimental conditions, the concentrations were of the order of a few micrograms per cubic centimeters, that is to say, 10^6 times higher than the aforementioned low concentrations (Table l) with particle sizes ranging from 20 to 100 nm. An average particle number of more than one thousand was always present within the plasma volume assuring LIBS detection for each laser shot and justifying ensemble averaging (i.e. accumulation of LIBS spectra) [11]. Within the concentration range probed during our LIBS experiment, the discrete nature of particles did not occasion particle miss (absence of analyte particles of the plasma) improving thereby signal-to-background ratio and repeatability. In future experiments, depending on particle concentration, further investigations could be necessary for spectra optimization either by increasing the number of accumulated spectra (in accordance with the time resolution wanted for process monitoring) or by improving data processing.

The second term of equation (5) evidences that stoichiometry relative uncertainty value strongly depends on a correct temperature determination and increases with increasing energy difference between the two upper state levels. The impact of the temperature uncertainty on stoichiometry determination is displayed on figure 9. This graph indicates that an error of around 1500 K in the temperature calculation induces a variation in stoichiometry determination of about 25 % (taking into account the variations of the

partition functions with temperature). Yet, an accurate determination of the plasma temperature remains difficult. The use of the Boltzmann's plot method for temperature calculation implies that all the lines used be not self-absorbed. This condition is not always easily achieved, though it is necessary to avoid calculation errors. These results actually highlight the need for a reliable tool allowing plasma characteristics determination with a better accuracy than by using Boltzmann's plot method or by measuring Stark broadening directly on a spectrum.

On the basis that laser-induced plasmas generated at atmospheric pressure are very close to the LTE state, the spectra emitted during LIBS experiments could actually be simulated using a LTE model. By comparing recorded spectra with synthetic spectra, characteristics such as electronic temperature, electronic density, plasma composition and subsequently stoichiometry can be determined using a model including diverse functionalities such as self-absorption modeling [27,28]. A correct fit guarantees plasma characteristic determination with uncertainties lower than with any other methods. Such model could be of great interest for future and advanced experiments concerning nanoparticle process control using LIBS. As the nanoparticle sampling flow concentration passing through the analysis cell can be varied at will by designing the right bypass line, the best laser-plasma-particle coupling should be investigated to approach as close as possible of the LTE state. Thus, stoichiometry of composite nanoparticles containing more than two elements could be determined with the best accuracy.

The results obtained in the course of our experiments point out the difficulty met when trying to obtain quantitative results without using calibration standards. In the framework of these experiments, a calibration free method was favored for this first attempt. The possibility of using a nanoparticle sampling flow as a reference for calibration is not ruled out. However, the method to be applied leading to the elaboration of a reliable nanoparticle sampling flow usable as a calibration standard remains to be determined.

5. Conclusion

Experiments aiming at demonstrating the feasibility of an on-line LIBS monitoring system allowing real time stoichiometry measurements during nanoparticle production by laser pyrolysis have been carried out. Part of the nanoparticle flow produced by the process was diverted through a flowing cell where the LIBS plasma was created. Time-resolved spectroscopic study of the laser-induced plasma was performed with

the aim of determining nanoparticle stoichiometry. Temporally-resolved electronic density and temperature measurements were obtained from Stark Broadening analysis and Boltzmann plot respectively. LTE validity was established and subsequently, stoichiometry was calculated using an equation relating line intensities to Boltzmann's law. Stoichiometry values found were in good agreement with the expected values. However, stoichiometry calculation proved to be sensitive to the uncertainty related to electronic temperature determination. A deeper study of the laser / plasma / nanoparticle coupling combined with LTE modeling could greatly enhance these promising results.

Acknowledgements

This work was supported by the Picardie Regional Council (France), the French Ministry of Environment and the FP6-Nanosafe2 European project.

References

[1] W. R. Cannon, S. C. Danforth, J. S. Haggerty and R. A. Marra, Sinterable Ceramic Powders from Laser-Driven Reactions: II, Powder Characteristics and Process Variables, J. Am. Ceram. Soc. 65 (1982) 330-335.

[2] P. Fichet, P. Mauchien, C. Moulin, Determination of impurities in uranium and plutonium dioxides by Laser-Induced Breakdown Spectroscopy, Appl. Spectrosc. 53 (1999) 1111-1117.

[3] P. Fichet, P. Mauchien, J.F. Wagner, C. Moulin, Quantitative elemental determination in water and oil by laser-induced breakdown spectroscopy, Anal. Chim. Acta 429 (2001) 269-278.

[4] L. Dudragne, Ph. Adam and J. Amouroux, Time-resolved laser-induced breakdown spectroscopy: application for qualitative and quantitative detection of fluorine, chlorine, sulfur and carbon in air, Appl. Spectrosc. 52 (1998) 1321-1327.

[5] D.A. Cremers and L.J. Radziemski, Detection of chlorine and fluorine in air by laser-induced breakdown spectroscopy, Anal. Chem. 55 (1983) 1252-1256.

[6] D.W. Hahn, M.M. Lunden, Detection and analysis of aerosol particles by laser-induced breakdown spectroscopy, Aerosol Sci. Technol. 33 (2000) 30-48.

[7] L.J. Radziemski, T.R. Loree, D. A. Cremers, N.M. Hoffman, Time-resolved laser-induced breakdown spectrometry of aerosols, Anal. Chem. 55 (1983) 1246-1252.

[8] R. Noll, H. Bette, A. Brysch, M. Krausharr, I. Mönch, L. Peter, V. Sturm, Laser-induced breakdown spectrometry – applications for production control and quality assurance in the steel industry, Spectrochim. Acta, Part B 56 (2001) 637-649.

[9] J. Gruber, J. Heitz, H. Strasser, D. Bäuerle, N. Ramaseder, Rapid in-situ analysis of liquid steel by laser-induced breakdown spectroscopy, Spectrochim. Acta, Part B 56 (2001) 685-693.

[10] A.I. Whitehouse, J. Young, I.M. Botheroyd, S. Lawson, C.P. Evans, J. Wright, Remote materials analysis of nuclear power station steam generator tubes by laser-induced breakdown spectroscopy, Spectrochim. Acta, Part B 56 (2001) 821-830.

[11] D.W. Hahn, W.L. Flower, K.R. Hencken, Discrete particle detection and metal emissions monitoring using laser-induced breakdown spectroscopy, Appl. Spectrosc. 51 (1997) 1836-1844.

[12] R.E. Neuhauser, U. Panne, R. Niessner, P. Wilbring, On-line monitoring of chromium aerosols in industrial exhaust streams by laser-induced plasma spectroscopy (LIPS), J. Anal. Chem. 364 (1999) 720-726.

[13] Meng-Dawn Cheng, Field measurement comparison of aerosl metals using aerosol beam focused laser-induced plasma spectrometer and reference methods, Talanta 61 (2003) 127-137.

[14] S.G. Buckley, H.A. Johnsen, K.R. Hencken and D.W. Hahn, Implementation of laser-induced breakdown spectroscopy as a continuous emission monitor for toxic metals, Waste Management 20 (2000) 455-462.

[15] J.E. Carranza, B.T. Fisher, G.D. Yoder, D.W. Hahn, On-line analysis of ambient air aerosols using laser-induced breakdown spectroscopy, Spectrochim. Acta, Part B 56 (2001) 851-864.

[16] G.A. Lithgow, A.L. Robinson, S.G. Buckley, Ambient measurements of metal-containing PM2.5 in an urban environement using laser-induced breakdown spectroscopy, Atmos. Environ. 38 (2004) 3319-3328.

[17] M. Cauchetier, O. Croix, M. Luce, M. Michon, J. Paris, S. Tistchenko, Laser synthesis of ultrafine powders, Ceram. Int. 13 (1987) 13-17.

[18] http://physics.nist.gov/PhysRefData/ASD/lines_form.html.

[19] Hans R. Griem, Principles of plasma spectroscopy, Cambridge University Press, 1997.

[20] A. W. Miziolek, V. Palleschi, I. Schechter, Laser-Induced Breakdown Spectroscopy, Cambridge University Press, 2006.

[21] N. Konjevic and W.L. Wiese, Experimental stark widths and shifts for spectral lines of neutral and ionized atoms, J. Phys. Chem. Ref. Data 19 (1990) 1307-1385.

[22] W.L. Wiese, D.E. Kelleher, D.R. Paquette, Detailed study of the Stark Broadening of Balmer Lines in a High-density Plasma, Phys. Rev. A: At., Mol., Opt. Phys. 6 (1972) 1132-1153.

[23] D.A. Cremers and L.J. Radziemski, Handbook of laser-induced breakdown spectroscopy, Wiley, 2006.

[24] J.E. Carranza and D.W. Hahn, Assessment of the upper particle size limit for quantitative analysis of aerosols using laser-induced breakdown spectroscopy, Anal. Chem. 74 (2002) 5450-5454.

[25] V. Hohreiter and D.W. Hahn, Calibration effects for laser-induced breakdown spectroscopy of gaseous sample streams: analyte response of gas-phase species versus solid-phase species, Anal. Chem. 77 (2005) 1118-1124.

[26] J.E. Carranza and D.W. Hahn, Plasma volume considerations for analysis of gaseous and aerosol samples using laser-induced breakdown spectroscopy, J. Anal. At. Spectrom. 17 (2002) 1534-1539.

[27] J. Hermann, C. Boulmer-Leborgne, and D. Hong, Diagnostics of the early phase of an ultraviolet laser-induced plasma by spectral line analysis considering self-absorption, J. Appl. Phys. 83 (1998) 691-696.

[28] J. Hermann and C. Dutouquet, Local thermal equilibrium plasma modeling for analyses of gas-phase reactions during reactive-laser ablation, J. Appl. Phys. 91 (2002) 10188-10193.

Figure caption

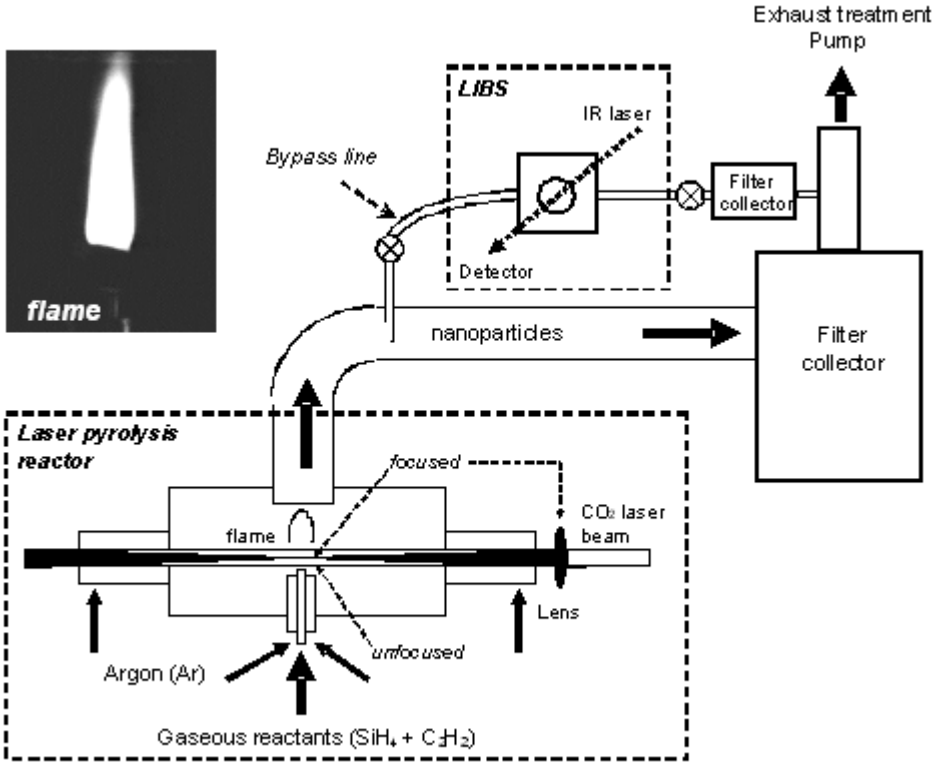

Figure 1. Laser pyrolysis reactor experimental set-up including the LIBS unit.

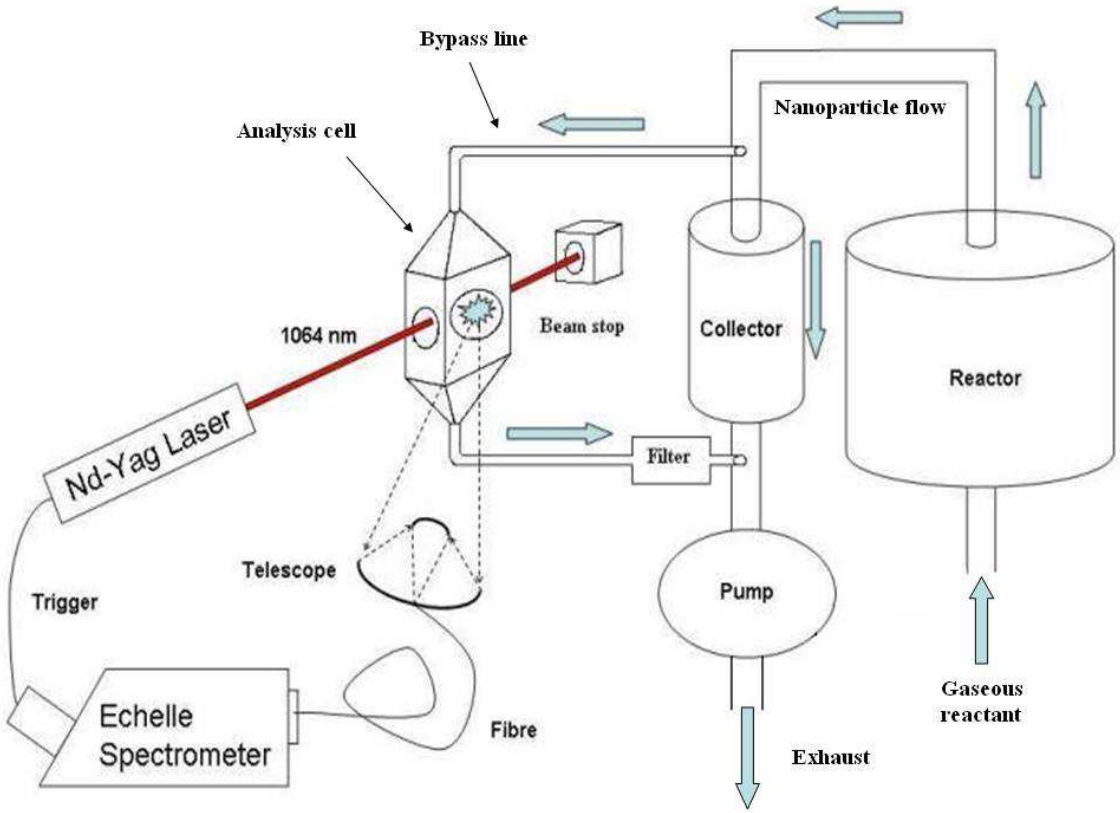

Figure 2. LIBS experimental set-up integrated into the laser pyrolysis process.

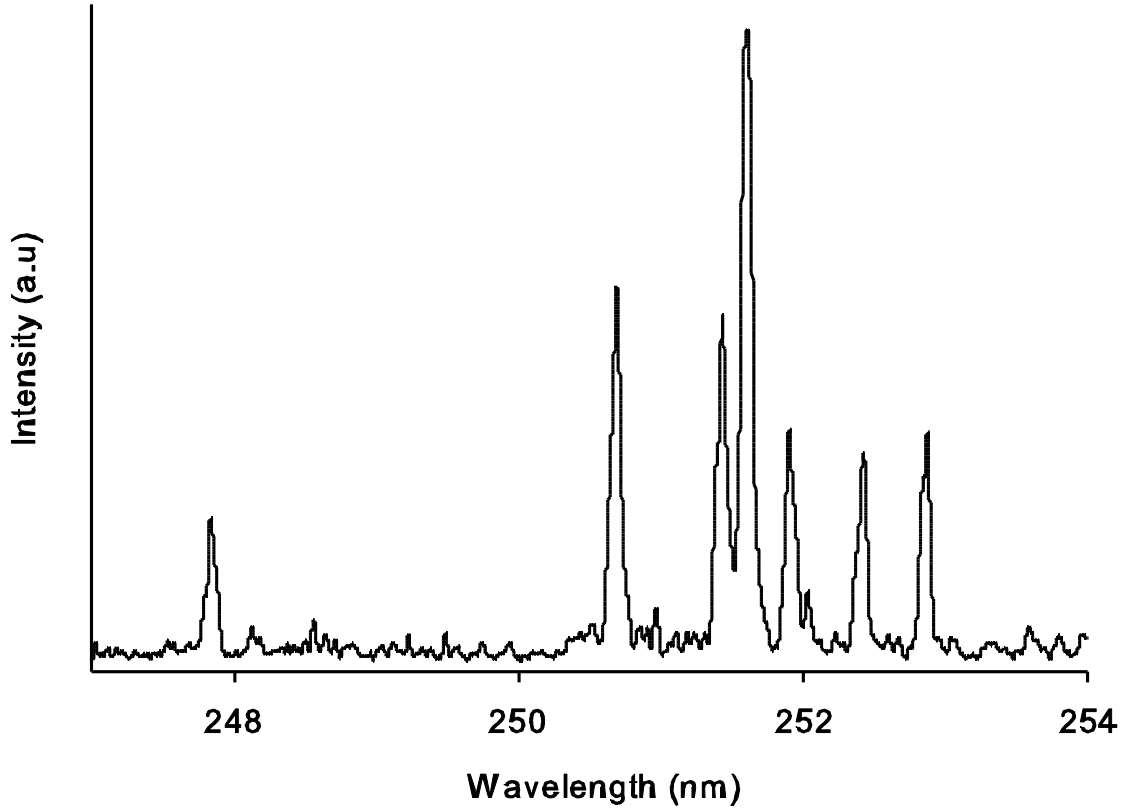

Figure 3. Spectrum recorded during vaporization of SiC_2 nanoparticles within the laser-induced plasma (time delay of 4.2 µs and an ICCD gate width of 2 µs). The line on the left is C I at 247.86 nm. The six other lines correspond to Si I at, from left to right: 250.69 nm, 251.43 nm, 251.61 nm, 251.92 nm, 252.41 nm and 252.85 nm.

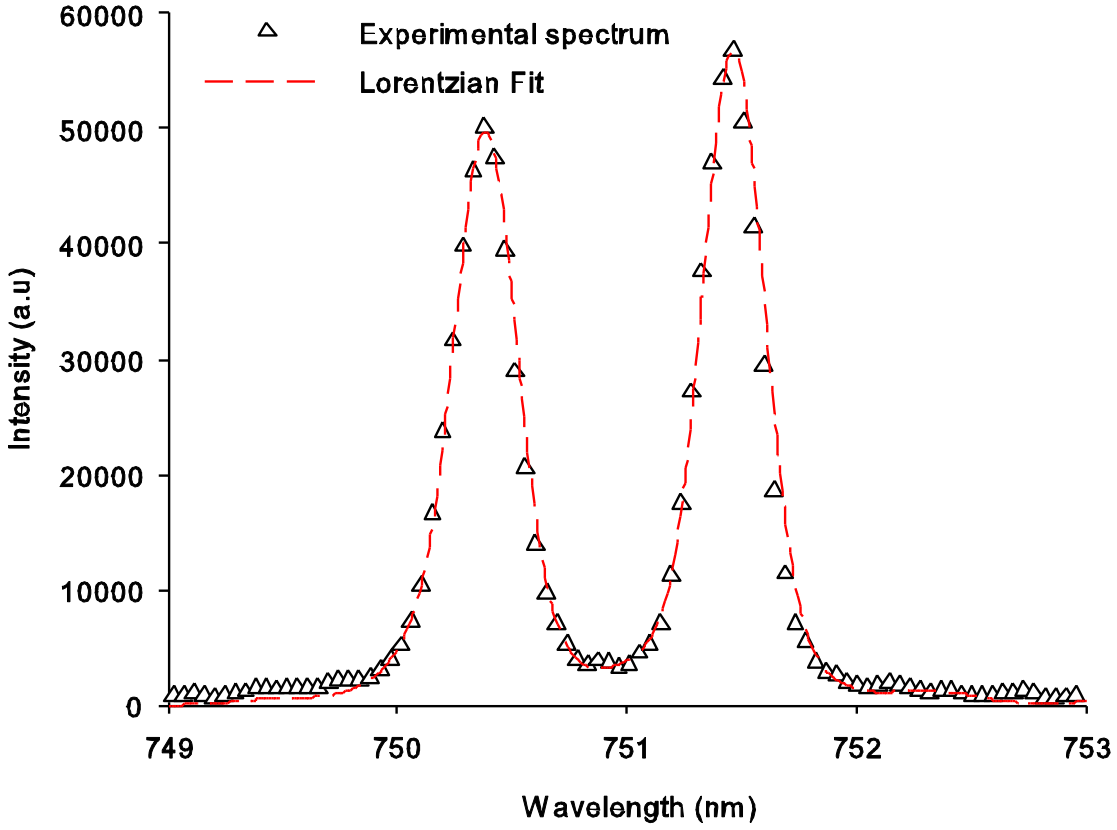

Figure 4. Example of simulated and experimental profiles of Stark-Broadened Ar lines at 750.386 and 751.465 nm used for electronic density measurements.

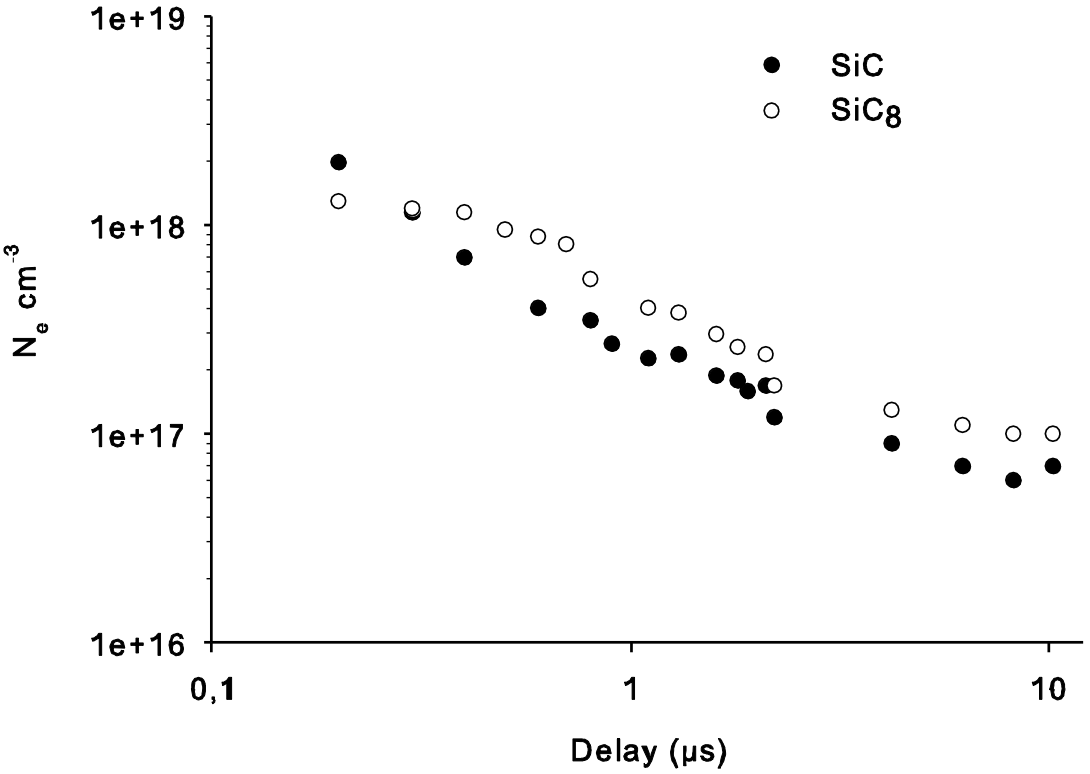

Figure 5. Temporal evolution of the electronic density during vaporization of SiC and SiC_8 nanoparticles within the laser-induced plasma generated in the argon background gas.

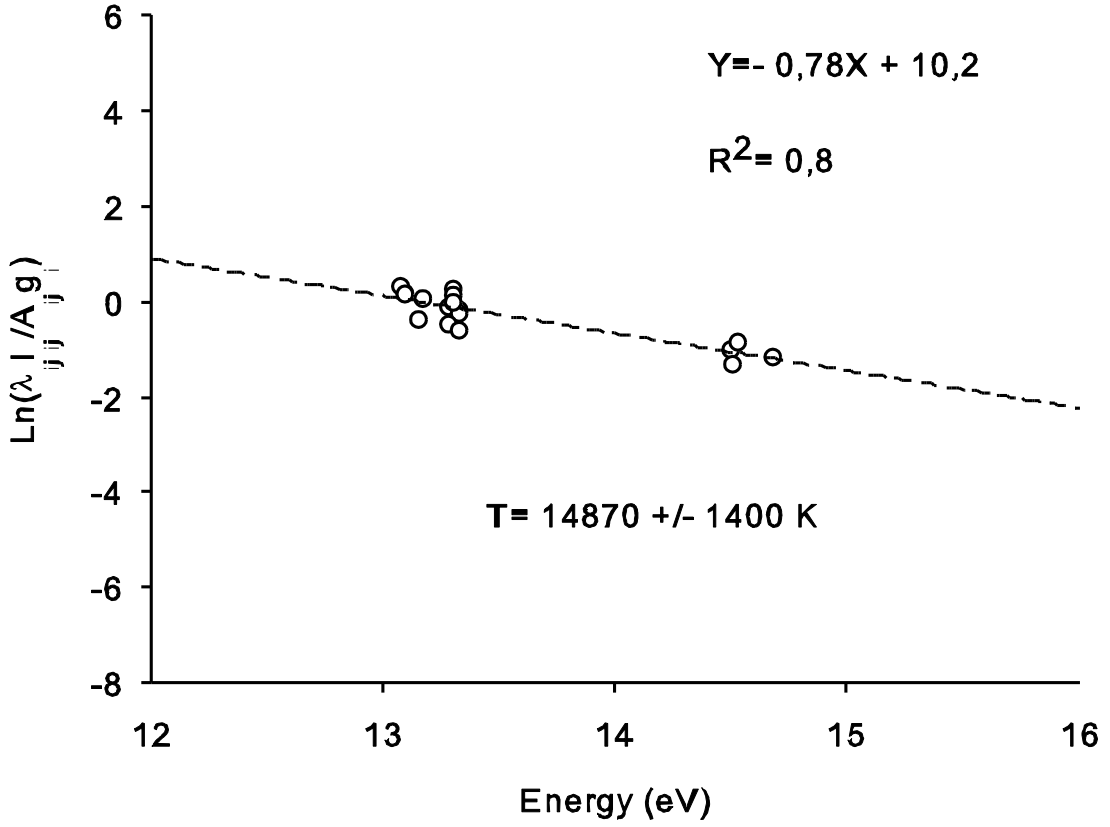

Figure 6. Example of Boltzmann plot obtained using argon lines (spectra recorded for time delay of 4.2 µs and gate width of 2µs) during SiC_2 Nanoparticle vaporization by the laser-induced plasma generated in the argon background gas.

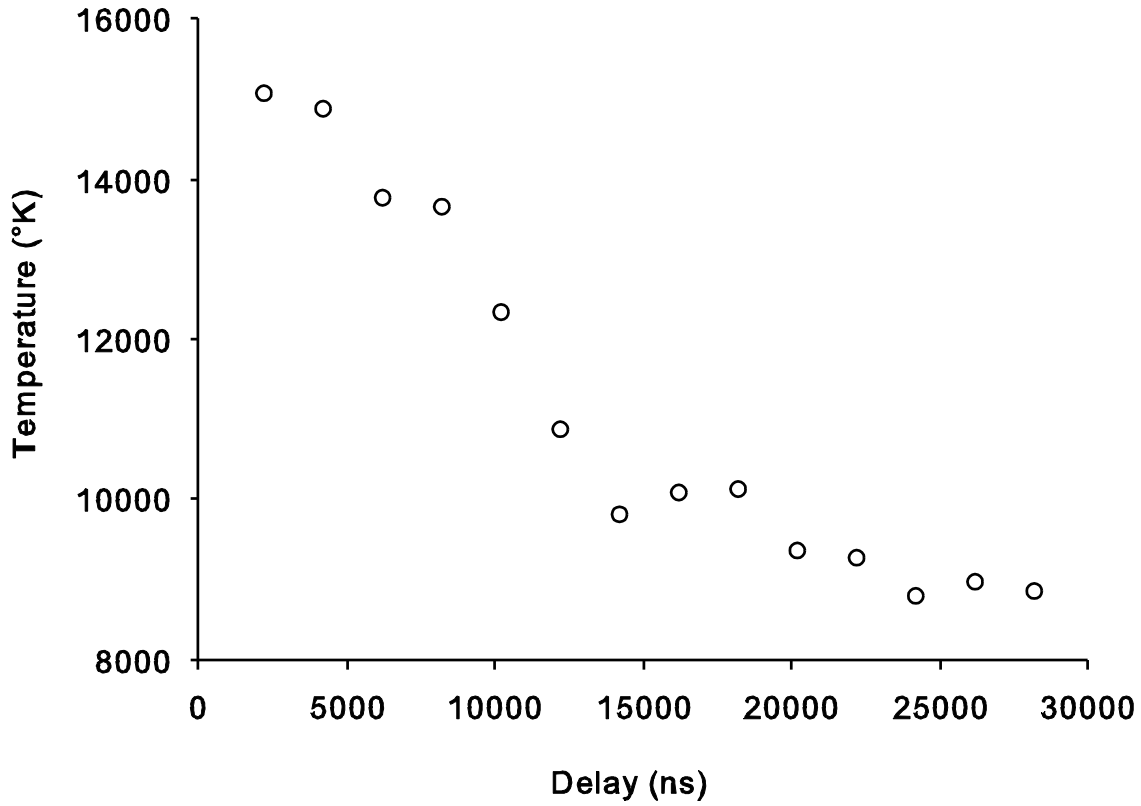

Figure 7. Temporal evolution of the electronic temperature during vaporization of SiC nanoparticles within the laser-induced plasma generated in the argon background gas.

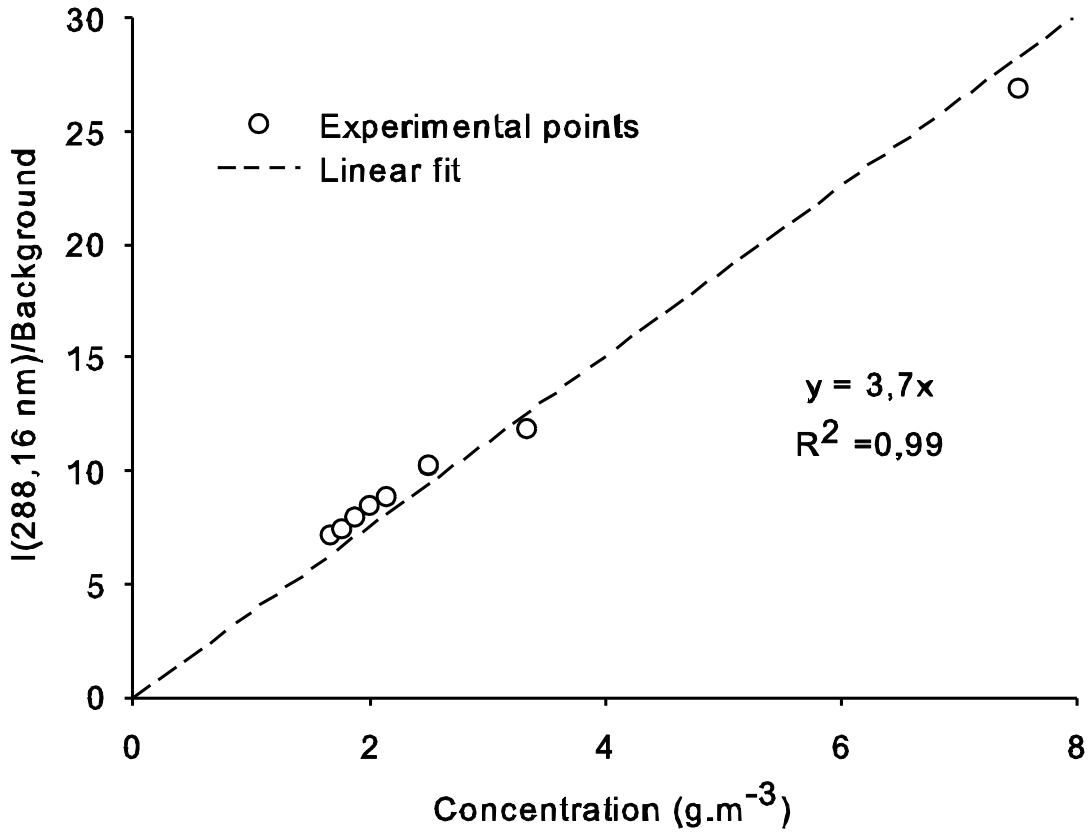

Figure 8. Si (288.157 nm) line intensity evolution as a function of Si nanoparticle concentration.

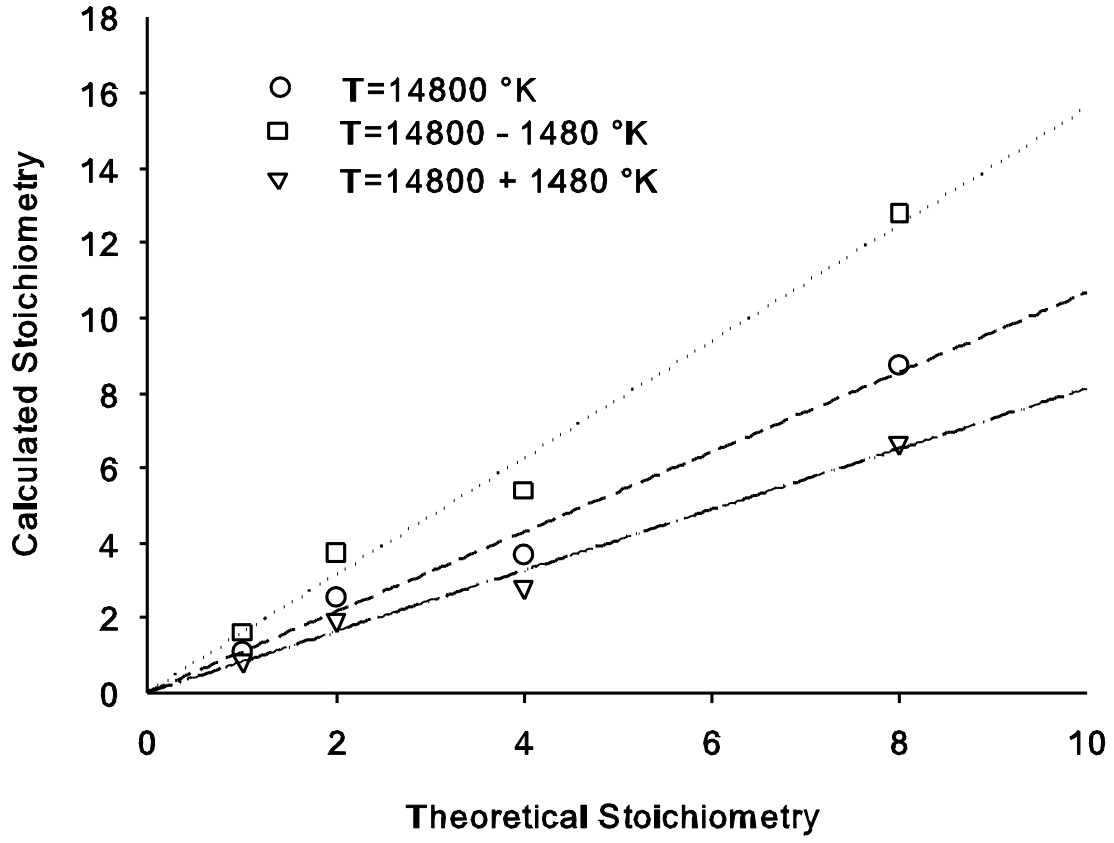

Figure 9. Influence of a 10% error in temperature determination on calculated stoichiometry.

Table 1. Reactants and argon flow rates, pressure within the chamber and laser power utilized during SiC_x nanoparticle synthesizing by laser pyrolysis. The theoretical nanoparticle-mass production values are indicated.

Theoretical compound	**SiH_4 Flow rate (l/min)**	**C_2H_2 Flow rate (l/min)**	**Ar Flow rate (l/min)**	**Theoretical Production (g/h)**	**Pressure (mbar)**	**Laser Power (W)**
SiC	0,8	0,4	170	86	950	1000
SiC_2	0,4	0,4	170	56	950	1000
SiC_4	0,2	0,4	170	41	970	1000
SiC_8	0,1	0,4	170	33	970	1000

Table 2. Wavelengths λ, transition probabilities $A_{ij} \times 10^7$, upper and lower level energies E_i and E_j and statistical weights of the upper states g_i of the 17 argon lines selected for the Boltzmann plots.

λ (nm)	**A_{ij} *10^7 (s^{-1})**	**E_i (eV)**	**E_j (eV)**	**g_i**
696,54	0,639	13,3279	11,5484	3
706,72	0,38	13,3022	11,5484	5
714,7	0,0625	13,2826	11,5484	3
727,29	0,183	13,3279	11,6236	3
738,39	0,847	13,3022	11,6236	5
763,51	2,45	13,1718	11,5484	5
794,81	1,86	13,2826	11,7232	3
801,47	0,928	13,0949	11,5484	5
810,36	2,5	13,1531	11,6236	3
811,53	3,31	13,0757	11,5484	7
826,45	1,53	13,3279	11,8281	3
840,82	2,23	13,3022	11,8281	5
842,46	2,15	13,0949	11,6236	5
419,10	0,0539	14,6806	11,7232	5
420,06	0,0967	14,4991	11,5484	7
426,62	0,0312	14,5289	11,6236	5
430,01	0,057	14,5061	11,6236	5

Table 3. Wavelengths λ, transition probabilities $A_{ij} \times 10^7$, upper level energies E_i, lower level energies E_j, statistical weights of the upper states g_i, of the Si and C selected lines for stoichiometry calculation. Z are the partition functions of Si and C in the neutral state calculated for temperature value T of 14800 K.

Element	**λ (nm)**	**A_{ij} *10^7 (s^{-1})**	**E_i (eV)**	**E_j (eV)**	**g_j**	**Z**	**T (K)**
Si	288,16	18,9	5,082	0,780	3	16,87	14800
C	247,85	3,4	7,684	2,684	3	11,51	14800

Table 4. Stoichiometry values calculated from equation (1).

Compound	Calculated Stoichiometry
SiC	1.1
SiC2	2.5
SiC4	3.7
SiC8	8.7